Chapter 2
In Vivo Imaging of Nicotinic Acetylcholine Receptors in the Central Nervous System

Masashi Ueda, Yuki Matsuura, Ryosuke Hosoda, and Hideo Saji

Abstract Nicotinic acetylcholine receptors (nAChRs) in the central nervous system are involved in higher brain function, i.e., memory, cognition, learning, among others. These receptors also exert various pharmacological effects, such as neuroprotection and antinociception. Therefore, elucidating the localization and/or expression level of nAChRs in the brain is useful to clarify functions regulated by nAChRs, under physiological and pathological conditions. "Molecular imaging" is a powerful tool that enables one to noninvasively obtain information from living subjects. Many signal types, such as, radiation, nuclear magnetic resonance, fluorescence, bioluminescence, and ultrasound, are commonly used for molecular imaging. Among them, nuclear medical molecular imaging, which uses radioactive imaging probes, has a great advantage due to its high sensitivity and the fact that it is a quantitative approach. Many nuclear medical imaging probes targeting nAChRs have been developed and some of them have successfully visualized nAChRs in the animal and human brain. Moreover, changes in nAChR density under pathological conditions have been detected in patients. This chapter summarizes the history and recent advance of nAChR imaging.

Keywords Molecular imaging · Radioactive probe · Positron emission tomography (PET) · Single-photon emission computed tomography (SPECT) · Nicotinic acetylcholine receptor · A-85380 · Alzheimer's disease

M. Ueda · Y. Matsuura · R. Hosoda
Graduate School of Medicine, Dentistry, and Pharmaceutical Science, Okayama University, Okayama, Japan
e-mail: mueda@cc.okayama-u.ac.jp; ph422132@s.okayama-u.ac.jp; p53u2dzh@s.okayama-u.ac.jp

H. Saji (✉)
Graduate School of Pharmaceutical Sciences, Kyoto University, Kyoto, Japan
e-mail: hsaji@pharm.kyoto-u.ac.jp

A. Akaike et al. (eds.), *Nicotinic Acetylcholine Receptor Signaling in Neuroprotection*, https://doi.org/10.1007/978-981-10-8488-1_2

2.1 Introduction

Nicotinic acetylcholine receptors (nAChRs) are pentameric ligand-gated ion channels. To date, a total of 17 subunits (α1–α10, β1–β4, γ, δ, and ε) have been identified (Nemecz et al. 2016) and nAChRs are formed from various combinations of these subunits. nAChRs are located in the central and peripheral nervous systems. In the central nervous system (CNS), nAChRs not only play a role in higher brain function, but also exert various pharmacological effects (Graef et al. 2011). The two major subtypes of nAChRs found in the mammalian CNS are heteromeric α4β2 nAChRs and homomeric α7 nAChRs (Terry et al. 2015). Therefore, assessing the localization and/or expression level of both subtypes in the CNS is of great interest since it enables us to elucidate the functions they regulate, under physiological and pathological conditions.

Molecular imaging is defined as the visualization, characterization, and measurement of biological processes at the molecular and cellular levels in humans and other living systems (Mankoff 2007). The localization and/or density of nAChRs in the human brain can be evaluated in a noninvasive way using molecular imaging techniques that specifically target nAChRs. Several imaging techniques, such as nuclear medical imaging, magnetic resonance imaging, optical imaging, and ultrasound, are commonly used for molecular imaging. Among them, nuclear medical molecular imaging, which uses radioactive imaging probes, is greatly advantageous due to its high sensitivity and the fact that it is a quantitative approach. The following imaging modalities are used for nuclear medical molecular imaging: positron emission tomography (PET) and single-photon emission computed tomography (SPECT). The principles and characteristics of PET and SPECT are summarized in the next section. Many probes for nAChR imaging using PET and SPECT have been developed. Some of them have successfully visualized nAChRs in the animal and human brain. Moreover, changes in nAChR density under pathological conditions have been detected in patients. The history and recent advances in molecular imaging that target nAChRs are summarized in later sections.

2.2 Nuclear Medical Imaging Modality

2.2.1 Positron Emission Tomography (PET)

PET is a nuclear medical imaging technique used to noninvasively acquire images that correspond to physiological and pathological functions in a living body.

Image acquisition using PET is initiated with the injection or inhalation of a positron-emitting radiopharmaceutical. The scan is started after a delay ranging from seconds to minutes to allow the transport to or uptake by the organ of interest. When the positron-emitting radioisotope decays, it emits a positron, which travels a

Table 2.1 Major radioisotopes used for positron emission tomography (PET) in a clinical setting

Radionuclide	Half-life
^{11}C	20.4 min
^{13}N	9.97 min
^{15}O	122 s
^{18}F	110 min

short distance before an electron-positron annihilation event occurs. This annihilation event produces two high-energy photons (511 keV) propagating in nearly opposite directions. Therefore, a PET detector targets the detection of this annihilation radiation of 511 keV. If two photons are detected within a short (~10 ns) time-window, an event is recorded along the line connecting the two detectors. Summing many such events results in quantities that approximate line integrals through the radioisotope distribution. No collimator is required for the PET scanner because collimation is done electronically, leading to relatively high sensitivity. If they are suitably calibrated, PET images yield quantitative estimates of the concentration of the radioactive imaging probe at specific locations within the body.

Non-radioactive carbon, nitrogen, oxygen, and fluorine generally consist in many compounds of biological interest and/or pharmaceuticals. Positron-emitting radionuclides of carbon, nitrogen, oxygen, and fluorine also exist, and can therefore be readily incorporated into a wide variety of useful radioactive imaging probes. Table 2.1 outlines several positron-emitting radioisotopes. This is, however, not an exhaustive list of positron-emitting radioisotopes, since many other positron-emitters have been recently produced on small medical cyclotrons with 10–20 MeV protons (Nickles 1991, 2003). The major disadvantage of PET is its cost. The short half-life of most positron emitting isotopes requires an on-site cyclotron, and the scanners themselves are significantly more expensive than single-photon cameras. Nevertheless, PET is widely used in research studies and there is growing clinical acceptance of its findings, primarily for the diagnosis and staging of cancer.

2.2.2 Single-Photon Emission Computed Tomography (SPECT)

Most of the clinical procedures using tracers to visualize specific tissue binding sites is performed using planar gamma-camera imaging, SPECT, and PET. Even after the recent explosive growth of clinical PET, the imaging of single-photon emitting radiopharmaceuticals with gamma cameras, both in planar mode or with SPECT, constitutes the largest fraction of clinical nuclear medicine. Many clinically established radiopharmaceuticals for SPECT are commercially available and are commonly used in imaging departments. Single-photon emitting radionuclides that are used as labels for tracer molecules often have sufficiently long half-lives to

Table 2.2 Major radioisotopes used for single-photon emission computed tomography (SPECT) in a clinical setting

Radionuclide	Half-life (h)	Gamma ray energy (keV)
^{67}Ga	78.3	93, 185, 300
^{99m}Tc	6.01	141
^{111}In	67.3	171, 245
^{123}I	13.3	159

allow the long-distance transportation. Alternatively, they can be obtained on site via generator systems. Tracers for SPECT can often be readily prepared on site using commercial reagents and kits. Therefore, in contrast with PET, the infrastructure associated with cyclotron production is not required.

A key element of the SPECT camera is its collimator design, which eliminates all photons that are not traveling normal to the detector surface. The presence of a collimator limits the direction of the incoming photons. Without this, it becomes extremely difficult to determine the origin of detected photons. The collimator design largely determines not only the overall spatial resolution but also the radiation count efficiency of the system. The challenge, however, is that increasing the efficiency by expanding hole size of the collimator, will result in a low resolution. Further, the low sensitivity and efficiency mean that studies must be acquired for a relatively long time to accumulate sufficient counts. The only alternative would be to increase the administered activity, but this is limited by the radiation dose administered to the patient.

Radionuclides for SPECT have a relatively longer half-life than those for PET. It is preferential to have medium gamma ray energy (100–200 keV) for SPECT imaging. It is well recognized that PET has a higher resolution, higher sensitivity, and a better quantitation capability than SPECT. However, more hospitals are equipped with SPECT scanners, making the use of SPECT as a routine procedure more practical. Commonly used radionuclides for SPECT imaging are listed in Table 2.2.

2.3 Imaging Probes for Nicotinic Acetylcholine Receptors

2.3.1 Imaging Probes for the α4β2 Subtype

Many efforts have been dedicated to the development of PET and SPECT probes targeting α4β2 nAChRs. Several probes have been successfully used to noninvasively image α4β2 nAChRs in the brains of healthy people and also detect changes in the expression of α4β2-nAChR in the brains of patients with various diseases. Based on the structure of the parent compound, the probes can roughly be classified as follows: nicotine, A-85380, and epibatidine. The characteristics of these probes are summarized in this section and their chemical structures are shown in Fig. 2.1.

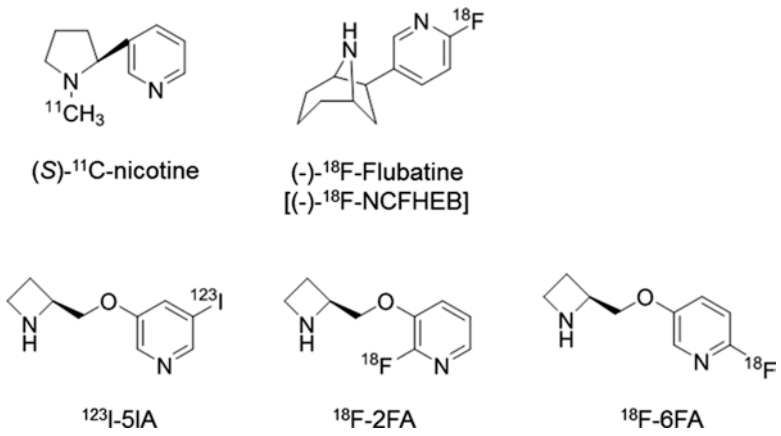

Fig. 2.1 Chemical structures of imaging probes targeting α4β2 nicotinic acetylcholine receptors (nAChRs)

2.3.1.1 Nicotine Derivatives

Nicotine was firstly selected as a parent backbone to visualize nAChRs. Saji et al. synthesized (*S*)- and (*R*)-^{11}C-nicotine by methylation of (*S*)- and (*R*)-nornicotine, respectively, using ^{11}C-methyl iodide. They then evaluated its biodistribution in mice. After an injection of (*S*)-^{11}C-nicotine, the order of regional uptake of radioactivity was as follows: cortex > thalamus > striatum > cerebellum. This uptake was displaced by the treatment of excess amount of unlabeled (*S*)-nicotine, but not by (*R*)-nicotine. (*R*)-^{11}C-nicotine showed less uptake and regional differences in the brain than (*S*)-^{11}C-nicotine (Saji et al. 1992). Nordberg et al. reported similar results using PET imaging in the rhesus monkey. After an injection of (*S*)-^{11}C-nicotine, the radioactivity in the brain peaked within 1–2 min and then rapidly declined. The highest accumulation of the probe was found in the occipital cortex and thalamus, while an intermediate and low accumulation of probe was found in the frontal cortex and white matter, respectively. Pretreatment with (*S*)-nicotine decreased the uptake of (*S*)-^{11}C-nicotine by 30%. In contrast, there was no regional difference in the distribution of (*R*)-^{11}C-nicotine (Nordberg et al. 1989). These findings indicated the specific binding of (*S*)-^{11}C-nicotine to nAChRs in vivo. However, it the amount of specific binding is low and results of (*S*)-^{11}C-nicotine in human PET studies are controversial.

2.3.1.2 A-85380 Derivatives

A-85380 [3-(2(*S*)-azetidinylmethoxy)pyridine] was developed in Abbott Laboratories. It showed 25-fold greater affinity to α4β2 nAChRs than nicotine did. The affinity of A-85380 to α4β2 nAChRs was comparable to that of epibatidine.

However, compared to the affinity of epibatidine, the affinities of A-85380 to other nicotinic receptor subtypes, such as α3β4, α7, and muscle type, were tenfold or less (Sullivan et al. 1996; Rueter et al. 2006). Therefore, A-85380 is a more α4β2-nAChR specific ligand than epibatidine. To date, radioiodinated and radiofluorinated A-85380 derivatives have been developed as SPECT and PET imaging probes, respectively, targeting α4β2 nAChRs.

A-85380-Derived SPECT Probe

The introduction of ^{123}I into five-position of pyridine ring of A-85380 yielded 5-[^{123}I] iodo-A-85380 (^{123}I-5IA) for SPECT imaging of α4β2 nAChRs. The affinity of $^{123/125}$I-5IA for α4β2 nAChRs was as extremely high (Ki = 10 pM) as that of epibatidine (Ki = 8 pM), when evaluated using rat brain homogenates. In contrast, the Ki values of 5IA for α3β4, α7, and muscle-type were 51, 250, and 1400 nM, respectively. Thus, the affinity ratios of α4β2-to-other subtype were calculated with 5100, 25,000, and 140,000, respectively (Mukhin et al. 2000). These results indicated that, despite the introduction of iodine to the parent backbone, ^{123}I-5IA maintained both the affinity and selectivity to α4β2 nAChRs.

In a biodistribution study in mice, the highest amount of ^{125}I-5IA accumulated in the thalamus (14.9% injected dose per gram of tissue [ID/g] at 60 min), while the accumulation was moderate in the cortex (8.5%ID/g at 60 min) and lowest in the cerebellum (2.4%ID/g at 60 min). Pretreatment with nAChR agonists (A-85380, (*S*)-nicotine, or cytisine) significantly reduced the accumulation of ^{125}I-5IA in the brain (Musachio et al. 1998). Saji et al. reported similar results in a study using rats. After injection of ^{125}I-5IA, the order of regional accumulation of radioactivity was followed: thalamus > cortex > striatum > cerebellum. This regional distribution was highly correlated with the nAChR density, which was determined using in vitro [^{3}H] cytisine binding. Further, SPECT imaging with ^{123}I-5IA clearly visualized the common marmoset brain. The radioactivity accumulation in the thalamus, which was higher than that in the cerebellum, decreased to the cerebellar level after the administration of cytisine (Saji et al. 2002). SPECT imaging of α4β2 nAChRs in the baboon brain was also successfully performed (Musachio et al. 1999; Fujita et al. 2000).

For the toxicity assessment of 5IA, behavior and physiological parameters (i.e., respiratory rate, heart rate, arterial blood pressure, and blood gas parameters) were examined. ICR mice that were injected intravenously 10 μg/kg of 5IA showed transient decrease in spontaneous locomotion. SD rats intravenously injected 5IA at 2 μg/kg and 5 μg/kg tended to have an increased respiratory rate. Conversely, no abnormal behavior was observed in mice injected 1 μg/kg of 5IA and their physiological parameters were maintained at normal levels. Therefore, the no observed effect level (NOEL) of 5IA was considered as 1 μg/kg (Ueda et al. 2004).

A-85380-Derived PET Probes

Two types of A-85380-based PET probes have been developed, i.e., 2-[^{18}F]fluoro-A-85380 (^{18}F-2FA) and 6-[^{18}F]fluoro-A-85380 (^{18}F-6FA). Both probes show promising properties for in vivo imaging of α4β2 nAChRs.

The Ki value of ^{18}F-2FA, which was determined in rat brain homogenates, using in vitro competitive binding assay with ^{3}H-epibatidine, was 46 pM (Koren et al. 1998). The radioactivity accumulation in the thalamus and cerebellum, at 60 min after intravenous injection of ^{18}F-2FA, was approximately 6%ID/g and 1%ID/g, respectively, (Horti et al. 1998). These values were approximately half a degree of ^{125}I-5IA, indicating lower brain penetration of ^{18}F-2FA compared to $^{123/125}$I-5IA. An in vivo blocking study performed in rats revealed that pretreatment with α4β2-nAChR ligands (nicotine, epibatidine, cytisine, or non-radioactive 2FA) reduced regional brain uptake of ^{18}F-2FA by 45–85%. Conversely, pretreatment with α7-nAChR ligand (methyllycaconitine) and 5-hydroxytryptamine-3 (5-HT_3)-receptor ligand (granisetron) did not affect the accumulation of ^{18}F-2FA (Doll et al. 1999). Therefore, it was proved that ^{18}F-2FA specifically bound to α4β2 nAChRs in vivo. Approximately twofold higher radioactivity was accumulated in the thalamus compared to the cerebellum in a PET imaging study performed using baboons (Valette et al. 1999). A toxicological study showed that intravenous injection of 2FA (0.8–10 μmol/kg) caused abnormal behavior in mice. However, a tracer dose (approximately 1 nmol/kg) of ^{18}F-2FA did not show signs of toxicity (Horti et al. 1998). Moreover, 2FA demonstrated no mutagenic properties evaluated by micronucleus and Ames tests (Valette et al. 2002).

The Ki value of ^{18}F-6FA was 25 pM determined by in vitro competitive binding assay using ^{3}H-epibatidine and rat brain homogenates (Koren et al. 1998). The brain uptake of ^{18}F-6FA was slight higher than that of ^{18}F-2FA. The radioactivity accumulation in the thalamus and cerebellum was approximately 8%ID/g and 1.5%ID/g, respectively, at 60 min after intravenous injection. Pretreatment with α4β2-nAChR ligands (nicotine and cytisine) reduced regional brain uptake of ^{18}F-6FA by 44–92% (Scheffel et al. 2000). There was a higher accumulation of ^{18}F-6FA in the thalamus than the cerebellum on PET imaging of the baboon brain. Compared with ^{18}F-2FA, the peak uptake was similar for both tracers. However, compared to ^{18}F-2FA, ^{18}F-6FA showed slightly faster kinetics (peak uptake in the thalamus was at 55–65 min and 60–80 min after the injection of ^{18}F-6FA and ^{18}F-2FA, respectively) and better contrast (thalamus-to-cerebellum ratio at 180 min was 2.5–3.5 and 1.9–2.1 for ^{18}F-6FA and ^{18}F-2FA, respectively) (Ding et al. 2000). However, one drawback of ^{18}F-6FA compared to ^{18}F-2FA may be its associated toxicity. Although a tracer dose (0.3 nmol/kg) of ^{18}F-6FA showed no signs of toxicity, higher doses (1.3 μmol/kg) of it induced increase in breathing and heart rate and severe seizures, while doses of 2.0 μmol/kg led to certain, immediate death. The approximate LD_{50} dose for intravenously injected 6FA was estimated to be 1.74 μmol/kg, which was approximately one-ninth that of 2FA (15 μmol/kg) in mice (Scheffel et al. 2000).

2.3.1.3 Epibatidine Derivatives

Epibatidine is an alkaloid that was isolated from the Ecuadorian poison frog *Epipedobates anthonyi* in 1992 (Fitch et al. 2010). It is one of the most potent nAChR agonists. Its agonistic potency is greater than that of A-85380 and nicotine (Anderson et al. 2000). Several epibatidine-based imaging probes have been developed, and one of them, (−)-^{18}F-flubatine, was recently applied in a first-in-human study.

(−)-^{18}F-flubatine is formally known as (−)-^{18}F-norchloro-fluoro-homoepibatidine [(−)-^{18}F-NCFHEB]. This probe was first reported in 2004. The binding affinity of (+)-enantiomer (Ki = 64 pM) and (−)-enantiomer (Ki = 112 pM) to human α4β2 nAChRs was five to ten times lower than that of epibatidine (Ki = 14 pM). However, given that the affinity of both enantiomers to human α3β4 nAChR was 65 times lower than that of epibatidine, this resulted in a 14-fold increase in α4β2 nAChR-specificity of flubatine compared to epibatidine (Deuther-Conrad et al. 2004). In a biodistribution study in mice, the brain uptake of (+)-^{18}F-flubatine (7.45%ID/g at 20 min) and (−)-^{18}F-flubatine (5.60%ID/g at 20 min) was greater than that of ^{18}F-2FA (3.20%ID/g at 20 min). Pre- and co-injection of 2FA decreased the brain uptake of (−)-^{18}F-flubatine by approximately 60%, indicating specific binding of (−)-^{18}F-flubatine to α4β2 nAChRs in vivo (Deuther-Conrad et al. 2008). The results of PET imaging with ^{18}F-flubatine in the porcine brain corroborated with the results of a biodistribution study performed in mice. The brain uptake was highest for (+)-^{18}F-flubatine, intermediate for (−)-^{18}F-flubatine, and lowest for ^{18}F-2FA, in all the examined regions (i.e., the thalamus, caudate/putamen, and cerebellum). Among these three probes, (−)-^{18}F-flubatine showed the fastest equilibrium of specific binding (Brust et al. 2008). Since the drawback of using ^{18}F-2FA in clinical PET studies is its slow kinetics, (−)-^{18}F-flubatine has the potential to overcome this challenge. PET imaging in the rhesus monkey revealed that the regional distribution of (−)-^{18}F-flubatine (i.e., thalamus > cortex/striatum > cerebellum) corroborated with the known distribution of α4β2 nAChRs: (Hockley et al. 2013). The toxicological effects of flubatine were evaluated by extended single dose toxicity studies. Wistar rats were intravenously injected with (−)-flubatine, at a dose of 24.8 μg/kg or more, and with (+)-flubatine, at a dose of 12.4 μg/kg or more, presented with symptoms that included tachypnea, labored breathing, and cyanosis. However, no symptoms were detected in rats injected (−)-flubatine and (+)-flubatine, at a dose of 6.2 μg/kg and 1.55 μg/kg, respectively. Therefore, the NOEL of (−)- and (+)-flubatine was considered as 6.2 and 1.55 μg/kg, respectively (Smits et al. 2014).

2.3.2 Imaging Probes for the α7 Subtype

Compared to α4β2-nAChR imaging probes, several promising probes were not as effective at targeting α7 nAChRs. However, the chemical structure of some probes that reached first-in-human studies is outlined in Fig. 2.2.

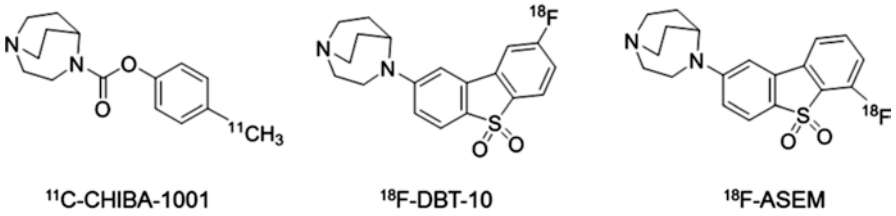

Fig. 2.2 Chemical structures of imaging probes targeting α7 nicotinic acetylcholine receptors (nAChRs)

^{11}C-CHIBA-1001 is the first α7-nAChR imaging probe to be used in humans (Toyohara et al. 2009). The IC_{50} value of CHIBA-1001 for ^{125}I-α-bungarotoxin, which is a selective antagonist for α7 nAChRs binding to rat brain homogenates, was 45.8 nM, indicating the high affinity of CHIBA-1001 to α7 nAChRs. The distribution of radioactivity matched the regional distribution of α7 nAChRs in a PET imaging study using ^{11}C-CHIBA-1001 in a conscious monkey. Moreover, the uptake of ^{11}C-CHIBA-1001 in the brain was inhibited by pretreatment with SSR180711, a selective α7-nAChR agonist, in a dose-dependent manner. It was however, not affected by A-85380, a selective α4β2-nAChR agonist (Hashimoto et al. 2008). The percentage of inhibition after treatment of SSR180711 (5 mg/kg) was approximately 40%.

Two dibenzothiophene-based probes that show a high affinity to α7 nAChRs were recently developed. These probes are ^{18}F-ASEM and ^{18}F-DBT-10, which is a *para*-isomer of ^{18}F-ASEM. The Ki value of ASEM for ^{125}I-α-bungarotoxin binding to the HEK293 cells stably expressing α7 nAChRs was 0.3 nM. A PET imaging study of the baboon clearly demonstrated its highest uptake in the thalamus and the lowest in the cerebellum. The uptake of ^{18}F-ASEM in the baboon brain was inhibited by the injection of SSR180711, in a dose-dependent manner (Horti et al. 2014). The percentage of inhibition following SSR180711 (5 mg/kg) treatment was approximately 80%, which was greater than that of ^{11}C-CHIBA-1001.

In a binding assay using SH-SY5Y cells stably expressing α7 nAChRs and ^{3}H-methyllycaconitine, ^{18}F-DBT-10 demonstrated a high affinity (Ki = 0.60 nM) for α7 nAChRs, which was comparable to ^{18}F-ASEM (Ki = 0.84 nM). PET imaging of the rhesus monkey brain clearly revelated its highest uptake in the thalamus and lowest update in the cerebellum. The brain uptake of ^{18}F-DBT-10 was inhibited by the administration of ASEM, in a dose-dependent manner (Hillmer et al. 2016b). Hillmer et al. directly compared the in vivo kinetic properties of ^{18}F-ASEM and ^{18}F-DBT-10 in identical rhesus monkeys and concluded that the two radiotracers were highly similar (Hillmer et al. 2017).

2.4 Nicotinic Acetylcholine Receptor Imaging in Human Brain

2.4.1 (S)-^{11}C-Nicotine

There are contrary reports regarding whether (*S*)-^{11}C-nicotine show specific binding to nAChRs in the human brain. Nybäck et al. performed (*S*)- and (*R*)-^{11}C-nicotine-PET in healthy male smokers and nonsmokers. Although (*S*)-^{11}C-nicotine demonstrated a higher uptake than (*R*)-^{11}C-nicotine, the co-administration of nonradioactive (*S*)-nicotine did not affect the time-activity curves of (*S*)-^{11}C-nicotine. A kinetic analysis based on a two-compartment model revealed that the brain uptake of (*S*)-^{11}C-nicotine was mainly determined using cerebral blood flow (CBF) (Nyback et al. 1994). Muzic et al. performed a similar study and demonstrated that the pharmacokinetics of (*S*)-^{11}C-nicotine could be well described using a two-compartment model, which was in accordance with the findings of Nybäck et al. Although the (*S*)-nicotine challenge induced a significant decrease in the distribution volume (DV) of (*S*)-^{11}C-nicotine, this decrease was small (Muzic et al. 1998). Therefore, both research groups concluded that (*S*)-^{11}C-nicotine was not a suitable tracer for PET studies of nAChRs in the human brain.

In contrast, Nordberg et al. developed a method for kinetic analysis of (*S*)-^{11}C-nicotine including compensation for the influence of CBF. They determined the CBF of each participant using ^{11}C-butanol- or ^{15}O-water-PET and compensated the rate constant of (*S*)-^{11}C-nicotine transport from tissue to blood using the CBF. In this analysis, a low rate constant corresponded to high (*S*)-^{11}C-nicotine binding in the brain. They revealed that the CBF-compensated rate constants were significantly and negatively correlated with cognitive function of patients with Alzheimer's disease (Nordberg et al. 1995; Kadir et al. 2006).

2.4.2 ^{123}I-5IA

Fujita et al. performed SPECT imaging and quantified the α4β2 nAChRs in the human brain using ^{123}I-5IA. A total of six healthy nonsmokers (two men and four women) participated in both a bolus and bolus-plus-constant infusion (B/I) study. Although the B/I study was not successfully applied, due to the slow kinetics of ^{123}I-5IA, regional DV values were successfully measured in the bolus study. The researchers applied one- and two-tissue compartment models to determine kinetic parameters of ^{123}I-5IA. The two-tissue compartment model provided better goodness-of-fit than the one-tissue compartment model, but the difference in the goodness-of-fit was relatively small. The obtained DV values were well-correlated between the two models. The DV values determined by two-tissue compartment model were highest in the thalamus (51 mL/cm^3), intermediate in putamen (27 mL/cm^3) and pons (32 mL/cm^3), slightly lower in cortical regions (17–20 mL/cm^3) (Fujita et al. 2003b).

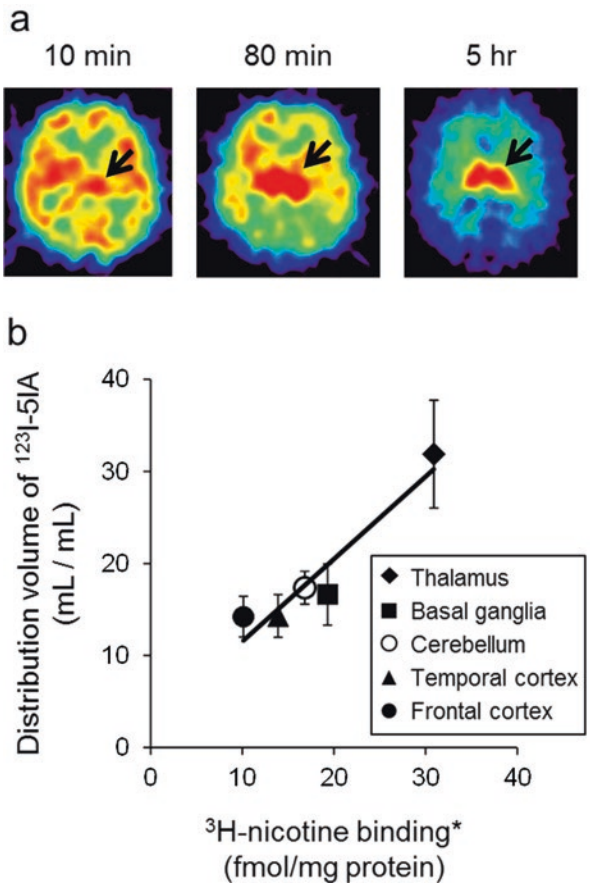

Fig. 2.3 Typical single-photon emission computed tomography (SPECT) images with ^{123}I-5IA and the correlation between distribution volumes of ^{123}I-5IA and reported nicotinic acetylcholine receptor (nAChR) density in the human brain. **(a)** Serial SPECT images obtained from a healthy human following the ^{123}I-5IA injection. Although blood flow-dependent distribution of radioactivity was observed at 10 min, the specificity of the radioactivity distribution for α4β2-nAChR in the thalamus (*the arrows*) could be distinguished in a time-dependent manner. **(b)** Correlation between distribution volumes (DV) of ^{123}I-5IA estimated using one-tissue compartment analysis and the reported nAChR density in the human brain. The Y-axis indicate DV values of ^{123}I-5IA and X-axis represent the α4β2 nAChR density in postmortem brains determined by ^{3}H-nicotine binding assay (Shimohama et al. 1986). The correlation coefficient was 0.95, indicating a highly significant correlation between the two parameters ($P < 0.05$)

Our research group also performed a similar study. Data from six healthy nonsmokers (five men and one woman), imaged using ^{123}I-5IA-SPECT, were analyzed with kinetic (one- and two-tissue compartment models) and Logan graphical tests (Logan et al. 1990). Figure 2.3a shows representative serial SPECT images. In contrast to the study performed by Fujita et al., two-tissue compartment analysis could not provide adequate rate constants. However, one-tissue compartment analysis could fit the data appropriately and regional DV values were successfully determined.

The obtained DV values were the highest in the thalamus (34 mL/g), intermediate in basal ganglia (17 mL/g) and brain stem (25 mL/g), and slightly lower in cortical regions (13–14 mL/g). These data correlated well with the nAChR densities, which was measured using ^{3}H-nicotine (Fig. 2.3b, R = 0.95, $P < 0.05$), indicating the validity of the analysis method. Moreover, similar DV values were successfully estimated using a graphical analysis (Mamede et al. 2004).

2.4.3 ^{18}F-2FA

Data from seven healthy male volunteers were compared using a compartmental kinetic analysis and Logan graphical analysis to quantify regional cerebral DV values of ^{18}F-2FA. PET scans were performed up to 240 min after the administration of ^{18}F-2FA, but the maximal concentration could not always be observed in the thalamus due to the slow kinetics of ^{18}F-2FA. Kinetic analysis revealed that the two-tissue compartment model was more accurate than the one-tissue compartment model to describe the PET data. The obtained DV values were the highest in the thalamus (15 mL/mL), and lower in the cerebellum, striatum, and cortical regions (5–7 mL/mL). These data were consistent with the known densities of nAChRs in the human brain that were measured using ^{3}H-epibatidine. The DV values obtained by the Logan graphical analysis were slightly lower than those obtained by the two-tissue compartmental kinetic analysis. This could be attributed to noise-induced bias. Therefore, the two-tissue compartmental kinetic analysis seems a more reliable method to estimate regional DV values of ^{18}F-2FA (Gallezot et al. 2005).

A simplified analysis method has been developed to easily quantify α4β2 nAChRs with ^{18}F-2FA-PET. Ten normal volunteers (six men and four women) were recruited for 2-h PET scan. Simplified DV values were defined as the ratio of radioactivity in the brain to that in arterial plasma at 90–120 min post-injection. Two-tissue compartment and Logan graphical analyses were also conducted on the data. DV values in the frontal cortex and cerebellum determined using the simplified method were significantly correlated with those calculated using the two-tissue compartment analysis and Logan graphical analysis ($r > 0.88$). Therefore, this simplified approach may be useful for quantifying cortical nAChRs and suitable for routine clinical application (Mitkovski et al. 2005).

2.4.4 (−)-^{18}F-Flubatine

A first-in-human PET study with (−)-^{18}F-Flubatine was reported in 2015 (Sabri et al. 2015). Dynamic PET imaging, lasting 270 min, was performed on 12 healthy male non-smoking participants, following a bolus injection of (−)-^{18}F-Flubatine intravenously. In humans, (−)-^{18}F-Flubatine is very stable against metabolism. Radiometabolite analysis of plasma demonstrated that almost 90% and 85% of

(−)-^{18}F-Flubatine existed in an intact form, at 90 min and 270 min after the injection, respectively. The tracer kinetics were well-described by both the one-tissue compartment and two-tissue compartment analyses, though the relative standard deviation of DV values determined by the two-tissue compartment analysis was much larger. The DV values were the highest in the thalamus (27 mL/cm^3), intermediate in regions like midbrain, striatum, and cerebellum (11–14 mL/cm^3), slightly lower in cortical regions (8–10 mL/cm^3), and lowest in the corpus callosum (6 mL/cm^3). These values were highly correlated with in vitro measurements of regional nAChR densities in the postmortem human brain using (±)-^{3}H-epibatidine (Marutle et al. 1998). DV values could be reliably estimated within 90 min for all the regions examined, demonstrating the faster kinetic property of (−)-^{18}F-Flubatine in humans.

Another research group performed (−)-^{18}F-Flubatine-PET in humans using a bolus-plus-infusion (B/I) paradigm, which could establish the true equilibrium between a probe in the plasma and at nAChRs in the brain. The DV values in the extrathalamic grey matter regions obtained from the B/I study corroborated well with those estimated by the two-tissue compartment analysis and multilinear analysis of the bolus data. The equilibrium in the thalamus, however, could not established under the B/I paradigm adopted in this study. The research group also assessed the probe's sensitivity to ACh fluctuations following physostigmine treatment in humans. PET acquisition with the B/I paradigm was performed and 1.5 mg of physostigmine was infused from 125 to 185 min. The DV values of (−)-^{18}F-Flubatine in the cortex, striatum, and cerebellum decreased by 2.8–6.5%. This difference was small since only a low dose to avoid peripheral side effects. However, this finding suggested that (−)-^{18}F-Flubatine is probably sensitive to changes in acetylcholine levels in humans (Hillmer et al. 2016a).

2.4.5 α7-nAChR Imaging Probes

^{11}C-CHIBA-1001 is the first α7-nAChR imaging probe to be used in humans. In the human brain, ^{11}C-CHIBA-1001 was widely distributed in all brain regions, including the cerebellum where uptake was low like in the monkey brain. This discrepancy could be attributed to species difference since it was in line with the result of a postmortem study, which demonstrated that the level of ^{125}I-α-bungarotoxin binding in the cerebellum was comparable to that in the cortex (Toyohara et al. 2009). Thus, this probe can be used to measure the occupancy rate of α7 nAChRs in the human brain. Ishikawa et al. examined the effect of tropisetron and ondansetron on PET imaging with ^{11}C-CHIBA-1001 in healthy non-smoking male participants. Tropisetron has a high affinity for both 5-HT$_3$ receptors and α7 nAChRs, while ondansetron only has a high affinity for 5-HT$_3$ receptors. Two serial PET scans were performed before and after an oral administration of these medications. Tropisetron decreased the total distribution volume of ^{11}C-CHIBA-1001 in the human brain, in a dose-dependent manner, while ondansetron had no effect (Ishikawa et al. 2011).

^{18}F-ASEM is another α7-nAChR imaging probe used in human PET imaging. The regional distribution of ^{18}F-ASEM in the brain was consistent with the expression of α7-nAChR in the post-mortem human brain. The cerebral cortex and putamen showed higher DV values (>20 mL/mL), while the caudate, cerebellum, and corpus callosum showed lower DV values (<15 mL/mL). Both one-tissue compartment and two-tissue compartment analyses fitted the data well and provided similar DV values. The average test-retest variability was 10.8%, indicating accurate estimation of DV values. However, this study was only performed on a limited number of participants (n = 2) (Wong et al. 2014). Another research group performed a ^{18}F-ASEM-PET in humans in 2017. In this study, one-tissue compartment analysis, rather than two-two compartment analysis, was the more suitable analysis method for the quantification of ^{18}F-ASEM kinetic parameters. However, since the one-tissue compartment analysis could produce a biased result in regions with high uptake of the probe, the authors finally chose a multilinear analysis method. The calculated DV values were higher in the cerebral cortex and putamen (>25 mL/cm^3) and lower in the caudate and cerebellum (19–21 mL/cm^3). The test-retest variability between the four participants was 11.7 ± 9.8% (Hillmer et al. 2017).

2.5 Alteration of Nicotinic Acetylcholine Receptor Density

2.5.1 Alzheimer's Disease (AD)

Memory impairment is the main symptom of AD, which is a progressive neurodegenerative disorder. Since nAChRs play a role in higher brain functions, such as cognition and memory, changes in the expression of nAChRs in AD is of great interest. Postmortem studies have demonstrated reduced activity of α4β2 nAChRs in patients with AD (Martin-Ruiz et al. 2000). O'Brien et al. recruited patients with AD, at the mild–moderate stages of illness and normal elderly controls, for a ^{123}I-5IA-SPECT study. Compared to that in the controls, significant reductions in ^{123}I-5IA binding were identified in the frontal cortex, striatum, and pons in patients with AD. There were no significant correlations with clinical or cognitive measures, which could be attributed to homogeneous stages of illness of the patients (O'Brien et al. 2007). In our study, DV values of ^{123}I-5IA in the cortical regions and thalamus in patients with AD were also decreased compared to that in age-matched healthy participants (Fig. 2.4) (Hashikawa et al. 2002; Ueda 2016).

AD is a progressive neurodegenerative disorder. The symptoms of AD are preceded by years of neurodegeneration in the brain. Mild cognitive impairment (MCI) is a clinically detectable initial stage of cognitive deficits and is considered as an intermediate state between healthy aging and AD. Therefore, if an nAChR abnormality is detected in patients with MCI, it will be an important biomarker at the earliest stage of the disease. It could consequently be used as a predictive biomarker to determine patients with MCI who are at risk for developing AD. Using ^{18}F-2FA-PET, Sabri et al. demonstrated a significant reduction in α4β2-nAChR availability

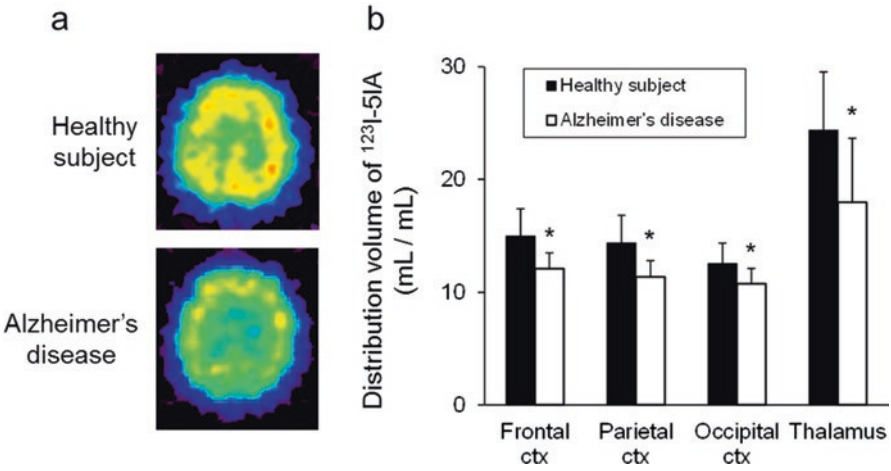

Fig. 2.4 Typical single-photon emission computed tomography (SPECT) images and mean distribution volumes of ^{123}I-5IA in age-matched healthy participant and patients with Alzheimer's disease (AD). (**a**) Representative ^{123}I-5IA SPECT images of an age-matched healthy participant and a patient with AD. (**b**) Mean distribution volumes of ^{123}I-5IA in age-matched healthy participants and patients with AD. Each bar represents an average of ten healthy participants and eight patients, and each error bar represents the SD (*$P < 0.05$ vs. healthy subject). *ctx* cortex

in the cortical regions, caudate head, and hippocampus, in patients with AD and MCI (Sabri et al. 2008). Kendziorra et al. also performed a ^{18}F-2FA-PET study on patients with MCI and AD, and age-matched healthy controls. The availability of α4β2-nAChR in the cortical regions, caudate, and hippocampus in patients with AD and MCI significantly decreased. More interestingly, compared to controls, patients with MCI who converted to AD showed a significantly low α4β2-nAChR availability in the above three regions. In contrast, the α4β2-nAChR availability of patients with MCI with stable cognitive course was also lower than that of controls, but the difference was not statistically significant (Kendziorra et al. 2011). However, other studies report conflicting results. The availability of α4β2 nAChRs in patients with MCI and at an early stage of AD were demonstrated to be maintained at a control level, using ^{123}I-5IA-SPECT (Mitsis et al. 2009) and ^{18}F-2FA-PET (Ellis et al. 2008).

2.5.2 Other Causes of Dementia

Although vascular dementia (VaD) is one of the most common causes of dementia in older people, the cholinergic involvement in VaD remains controversial. Some studies reported cholinergic loss (Gottfries et al. 1994), while others failed to demonstrate a cholinergic deficit in patients with VaD (Perry et al. 2005). Using ^{123}I-5IA-SPECT imaging, Colloby et al. demonstrated reductions in uptake of ^{123}I-5IA in the

dorsal thalamus and right caudate of patients with VaD, compared to that in age-matched healthy participants (Colloby et al. 2011). Another study revealed that, overall, ^{125}I-5IA binding in postmortem brains did not significantly differ between patients with VaD and age-matched healthy participants (Pimlott et al. 2004). However, an 11% reduction in ^{125}I-5IA binding was also demonstrated in the dorsal thalamus of patients with VaD. Nonetheless, the small sample size may have reduced statistical power.

Dementia with Lewy bodies (DLB) is the second most common cause of degenerative dementia in older people. It is well-known that cholinergic deficits are involved in DLB. O'Brien et al. performed a ^{123}I-5IA-SPECT study in patients with DLB and similarly aged controls. Compared to that in controls, the uptake of ^{123}I-5IA were significantly reduced in the frontal, striatal, temporal, and cingulate regions of patients with DLB (O'Brien et al. 2008). These findings were consistent with the findings obtained by a ^{125}I-5IA binding study using postmortem brains, where a significant reduction of ^{125}I-5IA binding was also observed in the striatum, entorhinal cortex, and substantia nigra (Pimlott et al. 2004).

2.5.3 Parkinson's Disease (PD)

In addition to the dopaminergic system, cholinergic neurons also play an important role in PD. Postmortem studies demonstrated widespread decrease in the expression of nAChR in the cortical and striatal regions of patients with PD (Rinne et al. 1991). Fujita et al. successfully detected this decrease in living patients with PD using ^{123}I-5IA-SPECT. A decrease of 3–9% and 15% in DV values was found in the cortical regions and thalamus, respectively, in patients with PD. However, this decrease was small and not statistically significant compared to healthy participants (Fujita et al. 2006). Oishi et al. also reported similar results using ^{123}I-5IA-SPECT. Patients with PD demonstrated a statistically significant decrease (20–25%) in the brainstem and frontal cortex, compared with that in the control group (Oishi et al. 2007). The difference in the SPECT scan procedure and/or withdrawal duration of antiparkinsonian medication may account for the discrepancy of the results obtained by the two studies.

Using ^{18}F-2FA PET, Meyer et al. estimated DV values in each brain region of patients with PD and healthy volunteers. They used the corpus callosum as a reference region, and the binding potential (BP) was calculated as follows: BP = (DV value in each brain region)/(DV value in the corpus callosum) – 1 (Brody et al. 2006). The BP values in patients with PD were significantly decreased (30–50%) in broad brain regions, such as cortical regions, caudate nucleus, midbrain, and cerebellum (Meyer et al. 2009).

2.5.4 Other Diseases

2.5.4.1 Alcohol Abuse

Although ethanol binding sites have not been identified in nAChRs, prolonged alcohol exposure reportedly increased agonist binding to α4β2 nAChRs (Robles and Sabria 2006). Therefore, Esterlis et al. examined α4β2-nAChR availability in heavy drinking nonsmokers and age- and sex-matched control nonsmokers (Esterlis et al. 2010). The nine participants who met the criteria for current alcohol abuse and two subjects who met criteria for current alcohol dependence were included in the ^{123}I-5IA-SPECT study. There were no significant differences in the availability of α4β2-nAChR between the two groups. However, as the authors noted, a larger study is warranted to explore effects of heavy alcohol drinking. In fact, recent PET and SPECT studies performed in nonhuman primates indicated a decrease in α4β2-nAChR availability after chronic ethanol consumption (Cosgrove et al. 2010; Hillmer et al. 2014).

2.5.4.2 Autosomal Dominant Nocturnal Frontal Lobe Epilepsy

Nocturnal frontal lobe epilepsy is a common non-lesional focal epilepsy (Provini et al. 1999). There are more than a hundred families with autosomal dominant nocturnal frontal lobe epilepsy (ADNFLE) and mutations in the genes encoding the α4 or β2 subunit of nAChR have been identified in several ADNFLE families (Picard and Scheffer 2005). Therefore, Picard et al. performed ^{18}F-2FA-PET imaging to measure the density of α4β2 nAChRs in eight ADNFLE patients and seven age-matched participants (Picard et al. 2006). Participants in both groups were nonsmokers. The DV values in patients with ADNFLE significantly increased in the epithalamus, ventral mesencephalon, and cerebellum, but decreased in the right dorsolateral prefrontal region. The downregulation of nAChR density in the prefrontal cortex is consistent with focal epilepsy involving the frontal lobe. The upregulation of nAChR density in the midbrain may be involved in the pathogenesis of ADNFLE through the role of cholinergic neurons ascending from the brainstem.

2.5.4.3 Major Depressive Disorders

Since hyperactivity of cholinergic neurons plays a pathophysiological role in depression (Dilsaver 1986), Saricicek et al. performed a ^{123}I-5IA-SPECT study in 23 non-smoking, medication-free patients with recurrent major depressive disorders (MDD) and 23 age- and sex-matched healthy controls (Saricicek et al. 2012). Compared to that in controls, patients with MDD had significantly lower availability of α4β2 nAChRs, across all the brain regions that were analyzed. However, there was no difference in the density of α4β2 nAChRs between patients with MDD and

healthy controls in the human postmortem brain. This discrepancy could be attributed to the competitive inhibition of excess amount of endogenous ACh, which could have resulted from the effect of cholinergic hyperactivity on ^{123}I-5IA accumulation.

2.5.5 Smokers

Many studies have demonstrated the upregulation of nAChRs occurred in both nicotine-treated animals (Yates et al. 1995) and postmortem brains of smokers (Buisson and Bertrand 2002). This upregulation is transient, however, and the nAChR density returns to baseline level after a period of abstinence from nicotine treatment (Pietila et al. 1998). Thus, the non-invasive detection of nAChR in smokers is important to monitor the dynamics of nAChR expression, i.e., upregulation during smoking and downregulation after smoking cessation.

Staley et al. were the first to noninvasively detect higher levels of α4β2 nAChRs in smokers (Staley et al. 2006). They performed ^{123}I-5IA-SPECT imaging and demonstrated an approximate 30% increase in DV values in the cortex and striatum of smokers after 7 days of abstinence. A similar upregulation was observed in ^{18}F-2FA-PET studies; the amount of increase, however, varied and could be attributed to differences in the extent of smoking and/or duration of smoking cessation before the imaging studies (Mukhin et al. 2008; Brody et al. 2013). Brody et al. reported an interesting finding that the upregulation of nAChRs was more pronounced in menthol cigarette smokers compared to non-menthol cigarette smokers (Brody et al. 2013). Heavy use of caffeine (i.e., an average of four cups of coffee per day) or marijuana (i.e., an average of 22 days of use per month) also affected the α4β2-nAChR density in smokers. An approximate 20–40% increase in DV values was observed in the prefrontal cortex, thalamus, and brainstem in smokers with heavy caffeine or marijuana use compared to smokers who were non-users (Brody et al. 2016). However, it is possible that the findings were independent of smoking, because the changes were not examined in nonsmokers with heavy caffeine or marijuana use.

Our research group successfully imaged the dynamic changes of nAChR expression during smoking cessation. We performed ^{123}I-5IA-SPECT imaging on six nonsmokers and ten smokers who had quit smoking for 4 h, 10 days, and 21 days. Five smokers in the 4-h group were included in either the 10-day or 21-day group. Compared to the DV values in nonsmokers, those in the brains of smokers decreased by approximately 35% in the 4-h group, but increased by approximately 25% in the 10-day group. The DV values in the 21-day group were comparable to those of nonsmokers, indicating that the density of α4β2 nAChRs had returned to the baseline level (Fig. 2.5) (Mamede et al. 2007). The decrease in the DV values in the 4-h

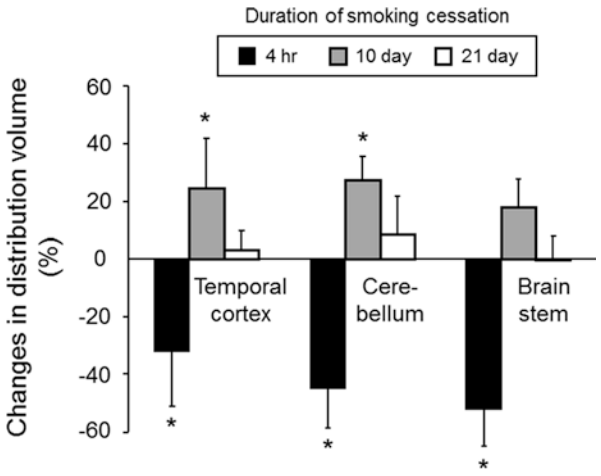

Fig. 2.5 Changes in the distribution volume of ^{123}I-5IA after smoking cessation. Compared to nonsmokers, the distribution volumes (DV) of ^{123}I-5IA of smokers at 4 h after ceasing smoking were significant lower, while those after 10-day cessation were significantly higher (*$P < 0.05$ vs. nonsmoker). The increased DV values returned to nonsmoker levels 21 days after ceasing smoking

group could be attributed to competitive inhibition of nicotine derived from tobacco on the binding of ^{123}I-5IA to nAChRs. A ^{18}F-2FA-PET study demonstrated that just one to two puffs of smoking resulted in 50% occupancy of α4β2 nAChRs for 3.1 h after smoking (Brody et al. 2006). Another study demonstrated the upregulation of α4β2-nAChR (approximately 25%) in smokers after 1 week of abstinence. The upregulation was maintained up to 4 weeks of abstinence (approximately 15% increase), but the DV values then returned to nonsmoker level by 6–12 weeks of abstinence (Cosgrove et al. 2009). Differences in the study cohorts could be a possible reason for discrepancy, since only men were included in the study performed by Mamede et al., while both men and women were included the study performed by Cosgrove et al.

The degree of upregulation of nAChRs in smokers is sex-dependent. Cosgrove et al. performed a ^{123}I-5IA-SPECT study on 26 male and 28 female smokers, and 26 male and 30 female age-matched nonsmokers. The availability of α4β2 nAChRs was significantly higher in the cortex, striatum, and cerebellum of male smokers compared to that in male nonsmokers. In contrast, there was no difference in α4β2-nAChR availability between female smokers and nonsmokers. The cortical and cerebellar α4β2-nAChR availability showed a significant negative correlation with the progesterone level in a SPECT imaging day. Therefore, female sex steroid hormones may have a role in the regulation of α4β2-nAChR availability (Cosgrove et al. 2012).

2.6 Nicotinic Acetylcholine Receptor Imaging in Mouse Brain

The recent availability of many transgenic mice lines that model human diseases have enabled researchers to better elucidate disease mechanisms and drug development. However, since many studies on imaging nAChRs have been performed in nonhuman primates and humans, technical issues have hampered imaging studies of nAChRs in the brain of small animals, especially mice. Mouse brains are too small to image clearly using PET and SPECT that are used clinically. However, recent advances have improved the sensitivity and spatial resolution of PET and SPECT, enabling small animal imaging, which has allowed researchers to clearly visualize organs of small rodents. Thus, nuclear medical translational research using transgenic mice has become possible and has aided elucidation of human disease pathology. We provided the first evaluation of SPECT imaging of α4β2 nAChRs in the mouse brain (Matsuura et al. 2016). A 60-min dynamic SPECT imaging session of α4β2 nAChRs in the mouse brain was performed using ^{123}I-5IA. For the accurate definition of regions of interest (ROIs), each mouse underwent magnetic resonance (MR) brain imaging prior to SPECT imaging. The ROIs were then positioned on the MR images prior to their application to SPECT images. The mean radioactivity for each ROI (i.e., cerebral cortex, striatum, hippocampus, thalamus, and cerebellum) was expressed as standardized uptake values (SUVs) and compared to the known distribution of α4β2 nAChRs in the mouse brain. ^{123}I-5IA-SPECT allowed clear visualization of the mouse brain. A significant positive correlation was observed between the SPECT signal intensity and the reported distribution of nAChRs, which was measured using [^{3}H]epibatidine (Marks et al. 1998) (Fig. 2.6, $R = 0.81$, $P < 0.0001$ at 30 min; $R = 0.72$, $P < 0.0001$ at 60 min). The accumulation of ^{123}I-5IA was significantly inhibited by pretreatment with (−)-nicotine. These findings indicated that ^{123}I-5IA SPECT images were α4β2 nAChR-specific, and that the signal intensity of the SPECT images can be used as an index of α4β2 nAChR density.

The binding of ^{123}I-5IA decreased after the administration of acetylcholinesterase inhibitors in the baboon (Fujita et al. 2003a) and human brain (Esterlis et al. 2013). Therefore, the sensitivity of ^{123}I-5IA-SPECT to changes in the amount of endogenous acetylcholine in the mouse brain was assessed. First, the effect of different concentrations of physostigmine on the cerebral accumulation of ^{125}I-5IA was analyzed using the evisceration method. Physostigmine reduced the accumulation of ^{125}I-5IA accumulation in all nAChR-rich regions, in a dose-dependent manner. Conversely, radioactivity levels in the blood increased in a dose-dependent manner. Physostigmine at a concentration of 0.75 mg/kg reduced the uptake of ^{125}I-5IA in the thalamus by 51% (Fig. 2.7a, $P < 0.01$). Next, ^{123}I-5IA-SPECT imaging was performed twice, i.e., before and after physostigmine pretreatment (0.75 mg/kg). Compared to the baseline measurements, SUVs in the thalamus was significantly reduced (by 38%) with the physostigmine pretreatment (Fig. 2.7b, $P < 0.05$).

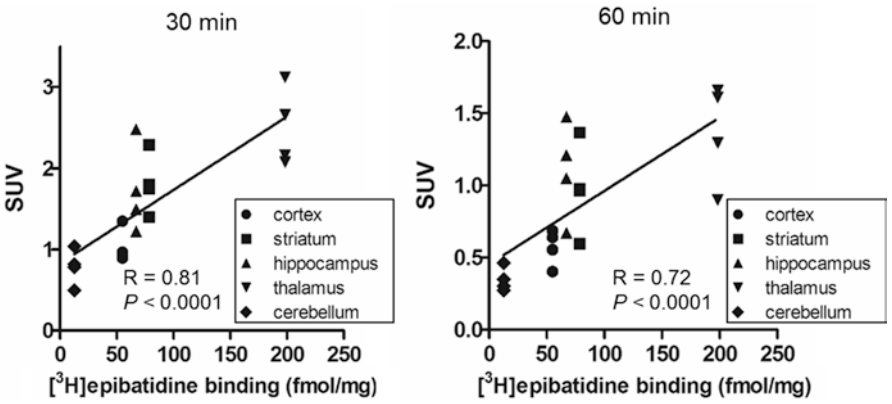

Fig. 2.6 Comparison of in vivo single-photon emission computed tomography (SPECT) analysis with the reported α4β2 nAChR density in the mouse brain. Correlation between in vivo radioactivity determined using SPECT/CT imaging and the reported α4β2 nAChR density in mouse brain. The Y-axis indicates the standardized uptake values (SUVs) in each brain region obtained at 30 min and 60 min after the ^{123}I-5IA injection. The X-axis represents the α4β2 nAChR density determined using [^{3}H]epibatidine binding assay (Marks et al. 1998). The correlation coefficient (R) was 0.81 and 0.72, at 30 min and 60 min, respectively, indicating a highly significant correlation between the two parameters ($P < 0.0001$)

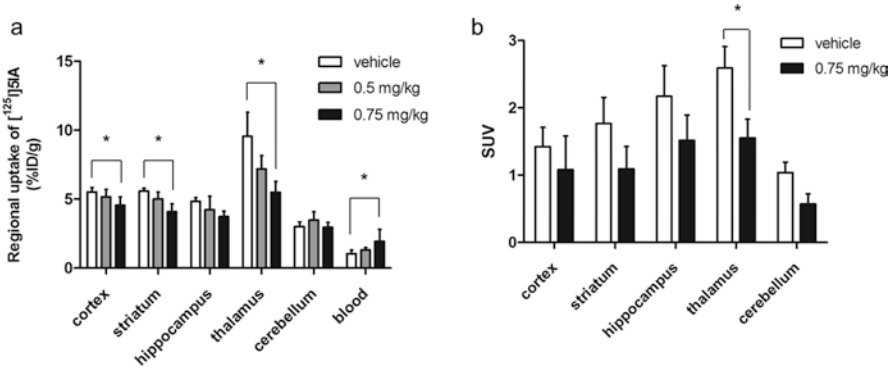

Fig. 2.7 The effect of physostigmine pretreatment on $^{123/125}$I-5IA accumulation. (**a**) The effect of different doses of physostigmine on ^{125}I-5IA accumulation in each brain region, as determined using the evisceration method. Each column represents average data from four mice and *error bars* represent the standard deviation (SD) (*$P < 0.05$, **$P < 0.01$ vs. vehicle). (**b**) The effect of physostigmine (0.75 mg/kg) on ^{123}I-5IA accumulation in each brain region was determined using the region of interest (ROI) analyses. Each *bar* represents the average of four mice and *error bars* represent the SD (*$P < 0.05$ vs. vehicle)

This suggested that SPECT images were affected by the increase in endogenous acetylcholinesterase caused by the administration of physostigmine. Therefore, ^{123}I-5IA-SPECT imaging may also be useful to evaluate the in vivo efficacy of acetylcholinesterase inhibitors in the mouse brain.

We also successfully detected the changes in nAChR density using ^{123}I-5IA-SPECT in the brains of frequently used mouse models of AD, i.e., the Tg2576 and APP/PS2 mice. Tg2576 mice overexpress human β-amyloid precursor protein (APP) with a familial AD gene mutation (Frautschy et al. 1998), while APP/PS2 mice are produced by crossbreeding Tg2576 mice with PS2 mice that overexpress human presenilin-2 (PS2) proteins carrying the Volga German Kindred mutation (N141I). The PS2 mutation reportedly accelerates AD-like phenotypes, such as the elevation of $A\beta_{1–40/1–42}$ levels, presence of amyloid plaques, and memory and learning defects, by several months, in Tg2576 mice (Toda et al. 2011). Consistent with the report by Toda et al. (2011), a novel object recognition (NOR) test demonstrated that the levels of cognition of APP/PS2 mice decreased at younger ages than those in Tg2576 mice. This test is based on the spontaneous tendency of rodents to spend more time exploring a novel object than a familiar one, and allows for the evaluation of cognition and recognition memory. The NOR test did not show significant differences in the cognitive ability between Tg2576 and wild-type mice at 13 months of age. Conversely, compared to wild-type mice, 12-month-old APP/PS2 mice exhibited a clear cognitive deficit. At first, ^{123}I-5IA-SPECT imaging was performed in Tg2576 and wild-type mice at 13 months of age. A 60-min dynamic SPECT/CT imaging was conducted following injection of ^{123}I-5IA into each mouse, via the tail vein. The distribution of radioactivity in each brain region was determined by ROI analysis and data were compared between Tg2576 and wild-type mice. ^{123}I-5IA-SPECT showed a higher signal in brains of Tg2576 mice than that in wild-type mice (Fig. 2.8a). SUVs in the thalamus were significantly higher than those in wild-type mice (22%, $P < 0.05$). SUVs in the cortex and hippocampus also tended to increase by 15% and 30%, respectively, although these differences were not statistically significant. [^{3}H]nicotine binding, which was evaluated in vitro using autoradiographic analysis at 7 days after SPECT/CT imaging, was also increased in Tg2576 mice compared to that in wild-type mice (Matsuura et al. 2016). These results suggested that nAChRs are upregulated in the Tg2576 mice at the age of 13 months.

Next, ^{123}I-5IA-SPECT imaging was performed in APP/PS2 and wild-type mice at the age of 12 months. In contrast to Tg2576 mice, the ^{123}I-5IA accumulation in APP/PS2 mice decreased in the cortex, hippocampus, and thalamus compared to that in wild-type mice ($P < 0.05$, Fig. 2.8b). The decrease in the nAChR density in the brains of APP/PS2 mice was supported by the reduction of α4 nAChRs protein levels, which was detected using Western blotting. These findings corroborated with a former study, which reported the loss of nAChRs in the cortex and hippocampus of patients with advanced AD (Guan et al. 2000). The reason for the discrepancy in α4β2 nAChR expression between Tg2576 and APP/PS2 mice, however, is unclear. It is possible that the pathology of Tg2576 mice at the age of 13 months represents a pre-AD state, while 12-month-old APP/PS2 mice might have the same extent of pathology seen in patients with AD. In fact, NOR memory and plaque deposition

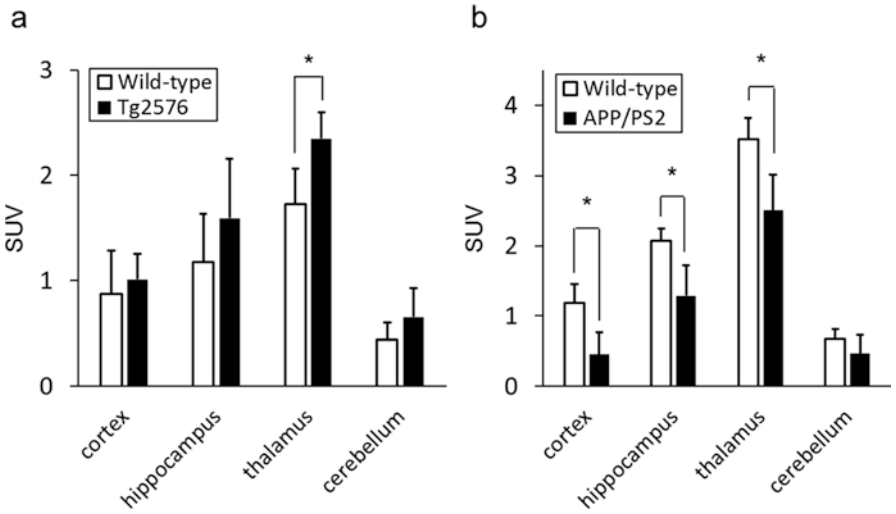

Fig. 2.8 Changes in the ^{123}I-5IA accumulation in brains of Tg2576 and APP/PS2 mice in vivo. In vivo ^{123}I-5IA-SPECT signal in brain regions of 13-month-old Tg2576 mice (**a**), 12-month-old APP/PS2 mice (**b**), and age-matched wild-type mice. ^{123}I-5IA accumulation was significantly increased in the thalamus of Tg2576 mice (*$P < 0.05$ vs. wild-type) and significantly decreased in the cortex, hippocampus, and thalamus of APP/PS2 mice (*$P < 0.05$ vs. wild-type). Each column represents averaged data from 4 to 5 mice and error bars represent the standard deviation

was not significantly different between Tg2576 and wild-type mice at the age of 13 months (Jacobsen et al. 2006). APP/PS2 mice, however, exhibited a clear cognitive deficit and severe plaque deposition in the cerebral cortex, at the age of 12 months. This hypothesis is also supported by the observation of the increase in ^{125}I-5IA accumulation in the hippocampus of APP/PS2 mouse at 6 months of age when the cognitive ability is still normal. These results suggested that the upregulation of α4β2 nAChRs might play a role in the mechanisms underlying neurodegeneration in patients with early-stage AD, who show increased Aβ expression. The discrepancy in the density of nAChR between several mouse models of AD would be an interesting focal point for research on AD pathology.

References

Anderson DJ, Puttfarcken PS, Jacobs I, Faltynek C (2000) Assessment of nicotinic acetylcholine receptor-mediated release of [^{3}H]-norepinephrine from rat brain slices using a new 96-well format assay. Neuropharmacology 39(13):2663–2672

Brody AL, Mandelkern MA, London ED et al (2006) Cigarette smoking saturates brain alpha 4 beta 2 nicotinic acetylcholine receptors. Arch Gen Psychiatry 63(8):907–915

Brody AL, Mukhin AG, La Charite J et al (2013) Up-regulation of nicotinic acetylcholine receptors in menthol cigarette smokers. Int J Neuropsychopharmacol 16(5):957–966

Brody AL, Hubert R, Mamoun MS et al (2016) Nicotinic acetylcholine receptor availability in cigarette smokers: effect of heavy caffeine or marijuana use. Psychopharmacology 233(17):3249–3257

Brust P, Patt JT, Deuther-Conrad W et al (2008) In vivo measurement of nicotinic acetylcholine receptors with [^{18}F]norchloro-fluoro-homoepibatidine. Synapse 62(3):205–218

Buisson B, Bertrand D (2002) Nicotine addiction: the possible role of functional upregulation. Trends Pharmacol Sci 23(3):130–136

Colloby SJ, Firbank MJ, Pakrasi S et al (2011) Alterations in nicotinic alpha4beta2 receptor binding in vascular dementia using ^{123}I-5IA-85380 SPECT: comparison with regional cerebral blood flow. Neurobiol Aging 32(2):293–301

Cosgrove KP, Batis J, Bois F et al (2009) Beta2-nicotinic acetylcholine receptor availability during acute and prolonged abstinence from tobacco smoking. Arch Gen Psychiatry 66(6):666–676

Cosgrove KP, Kloczynski T, Bois F et al (2010) Decreased Beta(2)*-nicotinic acetylcholine receptor availability after chronic ethanol exposure in nonhuman primates. Synapse 64(9):729–732

Cosgrove KP, Esterlis I, McKee SA et al (2012) Sex differences in availability of beta2*-nicotinic acetylcholine receptors in recently abstinent tobacco smokers. Arch Gen Psychiatry 69(4):418–427

Deuther-Conrad W, Patt JT, Feuerbach D, Wegner F, Brust P, Steinbach J (2004) Norchloro-fluoro-homoepibatidine: specificity to neuronal nicotinic acetylcholine receptor subtypes in vitro. Farmaco 59(10):785–792

Deuther-Conrad W, Patt JT, Lockman PR et al (2008) Norchloro-fluoro-homoepibatidine (NCFHEB) – a promising radioligand for neuroimaging nicotinic acetylcholine receptors with PET. Eur Neuropsychopharmacol 18(3):222–229

Dilsaver SC (1986) Pathophysiology of "cholinoceptor supersensitivity" in affective disorders. Biol Psychiatry 21(8–9):813–829

Ding Y, Liu N, Wang T et al (2000) Synthesis and evaluation of 6-[^{18}F]fluoro-3-(2(*S*)-azetidinylmethoxy)pyridine as a PET tracer for nicotinic acetylcholine receptors. Nucl Med Biol 27(4):381–389

Doll F, Dolci L, Valette H et al (1999) Synthesis and nicotinic acetylcholine receptor in vivo binding properties of 2-fluoro-3-[2(S)-2-azetidinylmethoxy]pyridine: a new positron emission tomography ligand for nicotinic receptors. J Med Chem 42(12):2251–2259

Ellis JR, Villemagne VL, Nathan PJ et al (2008) Relationship between nicotinic receptors and cognitive function in early Alzheimer's disease: a 2-[^{18}F]fluoro-A-85380 PET study. Neurobiol Learn Mem 90(2):404–412

Esterlis I, Cosgrove KP, Petrakis IL et al (2010) SPECT imaging of nicotinic acetylcholine receptors in nonsmoking heavy alcohol drinking individuals. Drug Alcohol Depend 108(1–2):146–150

Esterlis I, Hannestad JO, Bois F et al (2013) Imaging changes in synaptic acetylcholine availability in living human subjects. J Nucl Med 54(1):78–82

Fitch RW, Spande TF, Garraffo HM, Yeh HJ, Daly JW (2010) Phantasmidine: an epibatidine congener from the ecuadorian poison frog Epipedobates anthonyi. J Nat Prod 73(3):331–337

Frautschy SA, Yang F, Irrizarry M et al (1998) Microglial response to amyloid plaques in APPsw transgenic mice. Am J Pathol 152(1):307–317

Fujita M, Tamagnan G, Zoghbi SS et al (2000) Measurement of alpha4beta2 nicotinic acetylcholine receptors with [^{123}I]5-I-A-85380 SPECT. J Nucl Med 41(9):1552–1560

Fujita M, Al-Tikriti MS, Tamagnan G et al (2003a) Influence of acetylcholine levels on the binding of a SPECT nicotinic acetylcholine receptor ligand [^{123}I]5-I-A-85380. Synapse 48(3):116–122

Fujita M, Ichise M, van Dyck CH et al (2003b) Quantification of nicotinic acetylcholine receptors in human brain using [^{123}I]5-I-A-85380 SPET. Eur J Nucl Med Mol Imaging 30(12):1620–1629

Fujita M, Ichise M, Zoghbi SS et al (2006) Widespread decrease of nicotinic acetylcholine receptors in Parkinson's disease. Ann Neurol 59(1):174–177

Gallezot JD, Bottlaender M, Gregoire MC et al (2005) In vivo imaging of human cerebral nicotinic acetylcholine receptors with 2-^{18}F-fluoro-A-85380 and PET. J Nucl Med 46(2):240–247

Gottfries CG, Blennow K, Karlsson I, Wallin A (1994) The neurochemistry of vascular dementia. Dementia 5(3–4):163–167

Graef S, Schonknecht P, Sabri O, Hegerl U (2011) Cholinergic receptor subtypes and their role in cognition, emotion, and vigilance control: an overview of preclinical and clinical findings. Psychopharmacology 215(2):205–229

Guan ZZ, Zhang X, Ravid R, Nordberg A (2000) Decreased protein levels of nicotinic receptor subunits in the hippocampus and temporal cortex of patients with Alzheimer's disease. J Neurochem 74(1):237–243

Hashikawa K, Yoshida H, Inoue G et al (2002) Evaluation of nicotinic cholinergic receptors in the patients with Alzheimer disease by SPECT. J Nucl Med 43(5):63p–63p

Hashimoto K, Nishiyama S, Ohba H et al (2008) [^{11}C]CHIBA-1001 as a novel PET ligand for alpha7 nicotinic receptors in the brain: a PET study in conscious monkeys. PLoS One 3(9):e3231

Hillmer AT, Tudorascu DL, Wooten DW et al (2014) Changes in the alpha4beta2* nicotinic acetylcholine system during chronic controlled alcohol exposure in nonhuman primates. Drug Alcohol Depend 138:216–219

Hillmer AT, Esterlis I, Gallezot JD et al (2016a) Imaging of cerebral alpha4beta2* nicotinic acetylcholine receptors with (−)-[^{18}F]Flubatine PET: implementation of bolus plus constant infusion and sensitivity to acetylcholine in human brain. Neuroimage 141:71–80

Hillmer AT, Zheng MQ, Li S et al (2016b) PET imaging evaluation of [^{18}F]DBT-10, a novel radioligand specific to alpha7 nicotinic acetylcholine receptors, in nonhuman primates. Eur J Nucl Med Mol Imaging 43(3):537–547

Hillmer AT, Li S, Zheng MQ et al (2017) PET imaging of alpha7 nicotinic acetylcholine receptors: a comparative study of [^{18}F]ASEM and [^{18}F]DBT-10 in nonhuman primates, and further evaluation of [^{18}F]ASEM in humans. Eur J Nucl Med Mol Imaging 44(6):1042–1050

Hockley BG, Stewart MN, Sherman P et al (2013) (−)-[^{18}F]Flubatine: evaluation in rhesus monkeys and a report of the first fully automated radiosynthesis validated for clinical use. J Label Compd Radiopharm 56(12):595–599

Horti AG, Scheffel U, Koren AO et al (1998) 2-[^{18}F]Fluoro-A-85380, an in vivo tracer for the nicotinic acetylcholine receptors. Nucl Med Biol 25(7):599–603

Horti AG, Gao Y, Kuwabara H et al (2014) ^{18}F-ASEM, a radiolabeled antagonist for imaging the alpha7-nicotinic acetylcholine receptor with PET. J Nucl Med 55(4):672–677

Ishikawa M, Sakata M, Toyohara J et al (2011) Occupancy of alpha7 nicotinic acetylcholine receptors in the brain by tropisetron: a positron emission tomography study using [^{11}C] CHIBA-1001 in healthy human subjects. Clin Psychopharmacol Neurosci 9(3):111–116

Jacobsen JS, Wu CC, Redwine JM et al (2006) Early-onset behavioral and synaptic deficits in a mouse model of Alzheimer's disease. Proc Natl Acad Sci U S A 103(13):5161–5166

Kadir A, Almkvist O, Wall A, Langstrom B, Nordberg A (2006) PET imaging of cortical ^{11}C-nicotine binding correlates with the cognitive function of attention in Alzheimer's disease. Psychopharmacology (Berl) 188(4):509–520

Kendziorra K, Wolf H, Meyer PM et al (2011) Decreased cerebral alpha4beta2* nicotinic acetylcholine receptor availability in patients with mild cognitive impairment and Alzheimer's disease assessed with positron emission tomography. Eur J Nucl Med Mol Imaging 38(3):515–525

Koren AO, Horti AG, Mukhin AG et al (1998) 2-, 5-, and 6-Halo-3-(2(S)-azetidinylmethoxy)pyridines: synthesis, affinity for nicotinic acetylcholine receptors, and molecular modeling. J Med Chem 41(19):3690–3698

Logan J, Fowler JS, Volkow ND et al (1990) Graphical analysis of reversible radioligand binding from time-activity measurements applied to [*N*-^{11}C-methyl]-(−)-cocaine PET studies in human subjects. J Cereb Blood Flow Metab 10(5):740–747

Mamede M, Ishizu K, Ueda M et al (2004) Quantification of human nicotinic acetylcholine receptors with ^{123}I-5IA SPECT. J Nucl Med 45(9):1458–1470

Mamede M, Ishizu K, Ueda M et al (2007) Temporal change in human nicotinic acetylcholine receptor after smoking cessation: 5IA SPECT study. J Nucl Med 48(11):1829–1835

Mankoff DA (2007) A definition of molecular imaging. J Nucl Med 48(6):18N. 21N

Marks MJ, Smith KW, Collins AC (1998) Differential agonist inhibition identifies multiple epibatidine binding sites in mouse brain. J Pharmacol Exp Ther 285(1):377–386

Martin-Ruiz C, Court J, Lee M et al (2000) Nicotinic receptors in dementia of Alzheimer, Lewy body and vascular types. Acta Neurol Scand Suppl 176:34–41

Marutle A, Warpman U, Bogdanovic N, Nordberg A (1998) Regional distribution of subtypes of nicotinic receptors in human brain and effect of aging studied by (+/−)-[^{3}H]epibatidine. Brain Res 801(1–2):143–149

Matsuura Y, Ueda M, Higaki Y et al (2016) Noninvasive evaluation of nicotinic acetylcholine receptor availability in mouse brain using singlephoton emission computed tomography with [^{123}I]5IA. Nucl Med Biol 43(6):372–378

Meyer PM, Strecker K, Kendziorra K et al (2009) Reduced alpha4beta2*-nicotinic acetylcholine receptor binding and its relationship to mild cognitive and depressive symptoms in Parkinson disease. Arch Gen Psychiatry 66(8):866–877

Mitkovski S, Villemagne VL, Novakovic KE et al (2005) Simplified quantification of nicotinic receptors with 2[^{18}F]F-A-85380 PET. Nucl Med Biol 32(6):585–591

Mitsis EM, Reech KM, Bois F et al (2009) ^{123}I-5-IA-85380 SPECT imaging of nicotinic receptors in Alzheimer disease and mild cognitive impairment. J Nucl Med 50(9):1455–1463

Mukhin AG, Gundisch D, Horti AG et al (2000) 5-Iodo-A-85380, an alpha4beta2 subtype-selective ligand for nicotinic acetylcholine receptors. Mol Pharmacol 57(3):642–649

Mukhin AG, Kimes AS, Chefer SI et al (2008) Greater nicotinic acetylcholine receptor density in smokers than in nonsmokers: a PET study with 2-^{18}F-FA-85380. J Nucl Med 49(10):1628–1635

Musachio JL, Scheffel U, Finley PA et al (1998) 5-[I-125/123]Iodo-3(2(S)-azetidinylmethoxy) pyridine, a radioiodinated analog of A-85380 for in vivo studies of central nicotinic acetylcholine receptors. Life Sci 62(22.): PL):351–357

Musachio JL, Villemagne VL, Scheffel UA et al (1999) Synthesis of an I-123 analog of A-85380 and preliminary SPECT imaging of nicotinic receptors in baboon. Nucl Med Biol 26(2):201–207

Muzic RF Jr, Berridge MS, Friedland RP, Zhu N, Nelson AD (1998) PET quantification of specific binding of carbon-11-nicotine in human brain. J Nucl Med 39(12):2048–2054

Nemecz A, Prevost MS, Menny A, Corringer PJ (2016) Emerging molecular mechanisms of signal transduction in pentameric ligand-gated ion channels. Neuron 90(3):452–470

Nickles RJ (1991) A shotgun approach to the chart of the nuclides. Radiotracer production with an 11 MeV proton cyclotron. Acta Radiol Suppl 376:69–71

Nickles RJ (2003) The production of a broader palette of PET tracers. J Labelled Comp Radiopharm 46(1):1–27

Nordberg A, Hartvig P, Lundqvist H, Antoni G, Ulin J, Langstrom B (1989) Uptake and regional distribution of (+)-(*R*)- and (−)-(*S*)-*N*-[methyl-^{11}C]-nicotine in the brains of rhesus monkey. An attempt to study nicotinic receptors in vivo. J Neural Transm Park Dis Dement Sect 1(3):195–205

Nordberg A, Lundqvist H, Hartvig P, Lilja A, Langstrom B (1995) Kinetic analysis of regional (*S*) (−)^{11}C-nicotine binding in normal and Alzheimer brains – in vivo assessment using positron emission tomography. Alzheimer Dis Assoc Disord 9(1):21–27

Nyback H, Halldin C, Ahlin A, Curvall M, Eriksson L (1994) PET studies of the uptake of (*S*)- and (*R*)-[^{11}C]nicotine in the human brain: difficulties in visualizing specific receptor binding in vivo. Psychopharmacology (Berl) 115(1–2):31–36

O'Brien JT, Colloby SJ, Pakrasi S et al (2007) Alpha4beta2 nicotinic receptor status in Alzheimer's disease using ^{123}I-5IA-85380 single-photonemission computed tomography. J Neurol Neurosurg Psychiatry 78(4):356–362

O'Brien JT, Colloby SJ, Pakrasi S et al (2008) Nicotinic alpha4beta2 receptor binding in dementia with Lewy bodies using ^{123}I-5IA-85380 SPECT demonstrates a link between occipital changes and visual hallucinations. Neuroimage 40(3):1056–1063

Oishi N, Hashikawa K, Yoshida H et al (2007) Quantification of nicotinic acetylcholine receptors in Parkinson's disease with ^{123}I-5IA SPECT. J Neurol Sci 256(1–2):52–60

Perry E, Ziabreva I, Perry R, Aarsland D, Ballard C (2005) Absence of cholinergic deficits in "pure" vascular dementia. Neurology 64(1):132–133

Picard F, Scheffer I (2005) Recently defined genetic epileptic syndromes. In: Roger J, Bureau M, Dravet C, Genton P, Tassinari CA, Wolf P (eds) Epileptic syndromes in infancy, childhood and adolescence. John Libbey Eurotext, Montrouge, pp 519–535

Picard F, Bruel D, Servent D et al (2006) Alteration of the in vivo nicotinic receptor density in ADNFLE patients: a PET study. Brain 129(Pt 8):2047–2060

Pietila K, Lahde T, Attila M, Ahtee L, Nordberg A (1998) Regulation of nicotinic receptors in the brain of mice withdrawn from chronic oral nicotine treatment. Naunyn Schmiedeberg's Arch Pharmacol 357(2):176–182

Pimlott SL, Piggott M, Owens J et al (2004) Nicotinic acetylcholine receptor distribution in Alzheimer's disease, dementia with Lewy bodies, Parkinson's disease, and vascular dementia: in vitro binding study using 5-[^{125}I]-A-85380. Neuropsychopharmacology 29(1):108–116

Provini F, Plazzi G, Tinuper P, Vandi S, Lugaresi E, Montagna P (1999) Nocturnal frontal lobe epilepsy. A clinical and polygraphic overview of 100 consecutive cases. Brain 122(Pt 6):1017–1031

Rinne JO, Myllykyla T, Lonnberg P, Marjamaki P (1991) A postmortem study of brain nicotinic receptors in Parkinson's and Alzheimer's disease. Brain Res 547(1):167–170

Robles N, Sabria J (2006) Ethanol consumption produces changes in behavior and on hippocampal alpha7 and alpha4beta2 nicotinic receptors. J Mol Neurosci 30(1–2):119–120

Rueter LE, Donnelly-Roberts DL, Curzon P, Briggs CA, Anderson DJ, Bitner RS (2006) A-85380: a pharmacological probe for the preclinical and clinical investigation of the alphabeta neuronal nicotinic acetylcholine receptor. CNS Drug Rev 12(2):100–112

Sabri O, Kendziorra K, Wolf H, Gertz HJ, Brust P (2008) Acetylcholine receptors in dementia and mild cognitive impairment. Eur J Nucl Med Mol Imaging 35(Suppl 1):S30–S45

Sabri O, Becker GA, Meyer PM et al (2015) First-in-human PET quantification study of cerebral alpha4beta2* nicotinic acetylcholine receptors using the novel specific radioligand (−)-[^{18}F] Flubatine. Neuroimage 118:199–208

Saji H, Magata Y, Yamada Y et al (1992) Synthesis of (*S*)-*N*-[methyl-^{11}C]nicotine and its regional distribution in the mouse brain: a potential tracer for visualization of brain nicotinic receptors by positron emission tomography. Chem Pharm Bull (Tokyo) 40(3):734–736

Saji H, Ogawa M, Ueda M et al (2002) Evaluation of radioiodinated 5-iodo-3-(2(S)-azetidinylmethoxy)pyridine as a ligand for SPECT investigations of brain nicotinic acetylcholine receptors. Ann Nucl Med 16(3):189–200

Saricicek A, Esterlis I, Maloney KH et al (2012) Persistent beta2*-nicotinic acetylcholinergic receptor dysfunction in major depressive disorder. Am J Psychiatry 169(8):851–859

Scheffel U, Horti AG, Koren AO et al (2000) 6-[^{18}F]Fluoro-A-85380: an in vivo tracer for the nicotinic acetylcholine receptor. Nucl Med Biol 27(1):51–56

Shimohama S, Taniguchi T, Fujiwara M, Kameyama M (1986) Changes in nicotinic and muscarinic cholinergic receptors in Alzheimer-type dementia. J Neurochem 46(1):288–293

Smits R, Fischer S, Hiller A et al (2014) Synthesis and biological evaluation of both enantiomers of [^{18}F]flubatine, promising radiotracers with fast kinetics for the imaging of alpha4beta2-nicotinic acetylcholine receptors. Bioorg Med Chem 22(2):804–812

Staley JK, Krishnan-Sarin S, Cosgrove KP et al (2006) Human tobacco smokers in early abstinence have higher levels of beta2* nicotinic acetylcholine receptors than nonsmokers. J Neurosci 26(34):8707–8714

Sullivan JP, Donnelly-Roberts D, Briggs CA et al (1996) A-85380 [3-(2(S)-azetidinylmethoxy) pyridine]: in vitro pharmacological properties of a novel, high affinity alpha 4 beta 2 nicotinic acetylcholine receptor ligand. Neuropharmacology 35(6):725–734

Terry AV Jr, Callahan PM, Hernandez CM (2015) Nicotinic ligands as multifunctional agents for the treatment of neuropsychiatric disorders. Biochem Pharmacol 97(4):388–398

Toda T, Noda Y, Ito G, Maeda M, Shimizu T (2011) Presenilin-2 mutation causes early amyloid accumulation and memory impairment in a transgenic mouse model of Alzheimer's disease. J Biomed Biotechnol 2011:617974

Toyohara J, Sakata M, Wu J et al (2009) Preclinical and the first clinical studies on [^{11}C] CHIBA-1001 for mapping alpha7 nicotinic receptors by positron emission tomography. Ann Nucl Med 23(3):301–309

Ueda M (2016) Development of radiolabeled molecular imaging probes for in vivo analysis of biological function. Yakugaku Zasshi 136(4):659–668

Ueda M, Iida Y, Mukai T et al (2004) 5-[^{123}I]Iodo-A-85380: assessment of pharmacological safety, radiation dosimetry and SPECT imaging of brain nicotinic receptors in healthy human subjects. Ann Nucl Med 18(4):337–344

Valette H, Bottlaender M, Dolle F et al (1999) Imaging central nicotinic acetylcholine receptors in baboons with [^{18}F]fluoro-A-85380. J Nucl Med 40(8):1374–1380

Valette H, Dolle F, Bottlaender M, Hinnen F, Marzin D (2002) Fluoro-A-85380 demonstrated no mutagenic properties in in vivo rat micronucleus and Ames tests. Nucl Med Biol 29(8):849–853

Wong DF, Kuwabara H, Pomper M et al (2014) Human brain imaging of alpha7 nAChR with [^{18}F] ASEM: a new PET radiotracer for neuropsychiatry and determination of drug occupancy. Mol Imaging Biol 16(5):730–738

Yates SL, Bencherif M, Fluhler EN, Lippiello PM (1995) Up-regulation of nicotinic acetylcholine receptors following chronic exposure of rats to mainstream cigarette smoke or alpha 4 beta 2 receptors to nicotine. Biochem Pharmacol 50(12):2001–2008